

SHORTEST RECURRENCE PERIODS OF NOVAE

MARIKO KATO

Department of Astronomy, Keio University, Hiyoshi, Yokohama 223-8521, Japan

HIDEYUKI SAIO

Astronomical Institute, Graduate School of Science, Tohoku University, Sendai, 980-8578, Japan

IZUMI HACHISU

Department of Earth Science and Astronomy, College of Arts and Sciences, The University of Tokyo, 3-8-1 Komaba, Meguro-ku, Tokyo 153-8902, Japan

AND

KEN'ICHI NOMOTO

Kavli Institute for the Physics and Mathematics of the Universe (WPI), The University of Tokyo, 5-1-5 Kashiwanoha, Kashiwa, Chiba 277-8583, Japan and
Department of Astronomy, School of Science, The University of Tokyo, Bunkyo-ku, Tokyo 113-0033, Japan

submitted to the Astrophysical Journal

ABSTRACT

Stimulated by the recent discovery of the 1 yr recurrence period nova M31N 2008-12a, we examined shortest recurrence periods of hydrogen shell flashes on mass-accreting white dwarfs (WDs). We discuss the mechanism that yields a finite minimum recurrence period for a given WD mass. Calculating unstable flashes for various WD masses and mass-accretion rates, we identified the shortest recurrence period of about two months for a non-rotating $1.38 M_{\odot}$ WD with a mass-accretion rate of $3.6 \times 10^{-7} M_{\odot} \text{ yr}^{-1}$. One year recurrence period is realized for very massive ($> 1.3 M_{\odot}$) WDs with very high accretion rates ($> 1.5 \times 10^{-7} M_{\odot} \text{ yr}^{-1}$). We also present a revised stability limit of hydrogen shell burning, which will be useful for binary evolution calculations toward Type Ia supernovae.

Subject headings: nova, cataclysmic variables – stars: individual (M31N 2008-12a) – X-rays: binaries

1. INTRODUCTION

Recent discovery of the recurrent nova M31N 2008-12a attracts attention on novae with short recurrence periods (Darnley et al. 2014; Henze et al. 2014; Tang et al. 2014). M31N 2008-12a showed the shortest record of recurrence period of 1 yr, very rapid turn-on of the stable supersoft X-ray source (SSS) phase and high effective temperature (~ 100 eV) of the SSS phase, all of which indicate a very massive white dwarf (WD). Very massive WDs in recurrent novae are considered to be one of the candidates of Type Ia supernova (SN Ia) progenitors (Hachisu et al. 1999a,b; Hachisu & Kato 2001; Hachisu et al. 2010; Han & Podsiadlowski 2004; Kato & Hachisu 2012). SNe Ia play very important roles in astrophysics as a standard candle for measuring cosmological distances and as main producers of iron group elements in chemical evolution of galaxies. However, their immediate progenitors just before SN Ia explosions are still unclear. Thus, studies on novae with very short recurrence periods are essential to identify immediate progenitors of SNe Ia.

Many theoretical works on hydrogen shell flashes have been published. In general, short recurrence periods are obtained for very massive WDs with high mass-accretion rates. When the mass-accretion rate is larger than a certain value, nuclear burning is stable and no shell flashes occur (Sienkiewics 1975, 1980; Sion et al. 1979; Iben 1982; Nomoto et al. 2007; Wolf et al. 2013). The border of stable and unstable mass accretion rate is known as the stability line in the diagram of accretion rate vs. WD mass, i.e.,

\dot{M}_{stable} . For a given WD mass, a shortest recurrence period is obtained near the stability line. However, it is not well known whether this minimum recurrence period approaches a finite value or zero. Recently, Wolf et al. (2013) obtained numerically the recurrence periods near the stability line for various WD masses and showed that the minimum recurrence period is finite. However, the theoretical reason for the finite value is still unclear. Moreover, the stability line obtained by Wolf et al. (2013) with the time-evolution calculation slightly differs from that obtained with linear stability analysis (Sienkiewics 1975, 1980; Nomoto et al. 2007). Since the stability line is important in binary evolution calculations toward SNe Ia, we examine the stability line of shell flashes and clarify why there is a finite minimum value of recurrence period.

In the next section we explain the reason for finite minimum values of nova recurrence period. In Section 3, we present calculations of shell flashes on very massive WDs and numerically obtain minimum recurrence periods for various WD masses. We also present a revised stability line, which could be useful for calculations of binary evolution. In Section 4, we discuss some numerical calculations that resulted in shell flashes for mass-accretion rates above the stability line. Finally, we summarize our results in Section 5.

2. A LIMIT CYCLE OF HYDROGEN SHELL FLASHES AND FINITE RECURRENCE PERIODS

We first discuss a cycle of shell flashes by using hydrostatic envelope models. We calculated structures of hydrogen-rich envelopes on a mass-accreting WD by solving the equations of hydrostatic equilibrium, mass continuity, energy conservation, and energy transfer together with the equation of state

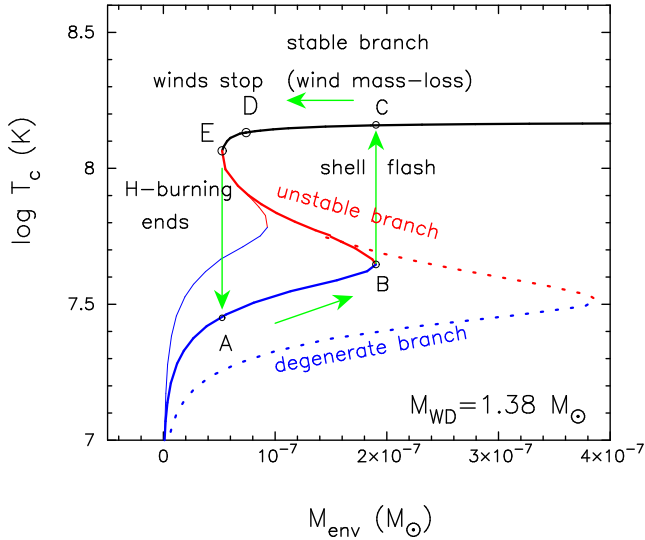


FIG. 1.— A schematic $M_{\text{env}} - \log T_c$ diagram for one cycle of nova outbursts on a $1.38 M_{\odot}$ WD with a given mass-accretion rate \dot{M} . We obtained numerically hydrogen-rich envelope equilibrium solutions on the WD. Here, T_c is the temperature at the bottom of the envelope and M_{env} is the envelope mass. We plot three cases of mass-accretion rates: above the stability line, i.e., $\dot{M} > \dot{M}_{\text{stable}}$ (thin solid line); somewhat below the stability line, i.e., $\dot{M} < \dot{M}_{\text{stable}}$ (thick solid line); much below the stability line, i.e., $\dot{M} \ll \dot{M}_{\text{stable}}$ (dotted line). In the case of thick solid line, the WD starts accretion around point A and increases the envelope mass. When it reaches a turning point B, a shell flash begins. So the ignition mass is defined as $M_{\text{ig}} = M_{\text{env}}(\text{B})$. Then the envelope expands and reaches point C. After optical maximum at point C, the envelope mass decreases owing to wind mass-loss and nuclear burning. The optically thick winds stop at point D. Hydrogen burning ends at point E and the envelope quickly cools down toward point A. In this S-shape sequence from point A to B, B to E, and E to C through D, the lower branch (blue line from A to B) represents a degenerate envelope and the middle branch (red line from B to E) does an unstable envelope for nuclear burning. The upper branch (black line from E to C) represents an extended envelope after optical maximum, where nuclear burning is stable. For the lower mass-accretion rate (dotted line), its degenerate branch is cooler owing to smaller gravitational energy release, and hence the ignition mass is larger. For the higher mass-accretion rate, the ignition mass is smaller. We found that the width of this limit cycle, $\Delta = M_{\text{env}}(\text{B}) - M_{\text{env}}(\text{E})$, does not vanish even for very high mass-accretion rates above the stability line (thin solid line). This is the reason for a minimum recurrence period of $t_{\text{rec}}^{\text{min}} = \Delta / \dot{M}_{\text{stable}}$. See text for detail.

for degenerate matter (Eggleton et al 1973). We used OPAL radiative opacities (Iglesias & Rogers 1996). The equation of energy conservation includes terms of nuclear burning, gravitational energy release, and radiative loss. For gravitational energy release we calculated so-called homologous compressional heating, ϵ_g^h , by accretion in a quasi-steady state on the q -coordinate ($q \equiv M_r/M$), which is in proportion to the mass-accretion rate \dot{M} (see, e.g., Neo et al. 1977; Kato 1980, 1982).

Figure 1 schematically depicts one cycle of shell flashes in the $M_{\text{env}} - \log T_c$ diagram for a $1.38 M_{\odot}$ WD with a given mass-accretion rate of \dot{M} , where M_{env} is the envelope mass and T_c is the temperature at the bottom of hydrogen-rich envelope. We connect each envelope solution by a line. Here, we plot three cases of mass-accretion rates: above the stability line, i.e., $\dot{M} > \dot{M}_{\text{stable}}$ (thin solid line); somewhat below the stability line, i.e., $\dot{M} < \dot{M}_{\text{stable}}$ (thick solid line); much below the stability line, i.e., $\dot{M} \ll \dot{M}_{\text{stable}}$ (dotted line). It should be noted that the exact stability line will be determined by time-dependent calculation of shell flashes in Section 3.2. The hydrostatic solutions form an S-shape sequence. The lowest branch, dubbed “degenerate branch,” represents a geometri-

cally thin envelope in which the radiative energy loss is mostly balanced with the gravitational energy release because the energy generation by nuclear burning is very small. In the middle branch, dubbed “unstable branch,” the energy loss is balanced with the energy generation of hydrogen burning and the gravitational energy release (ϵ_g^h). The energy generation by nuclear burning is comparable to or even dominates the gravitational energy release. Hydrogen shell burning on the middle branch is unstable. The upper branch, dubbed “stable branch,” represents an expanded phase of nova outburst. In the right side to point D, optically thick winds occur and each envelope solution is constructed including wind mass-loss (Kato & Hachisu 1994). Hydrogen shell-burning is stable on this branch (Kato 1983).

In the case of thick solid line ($\dot{M} < \dot{M}_{\text{stable}}$) in Figure 1, a mass-accreting WD begins its evolution from somewhere on the degenerate branch around point A. The envelope mass increases with time due to accretion and moves rightward along the degenerate branch. After it reaches the turning point of the degenerate branch (point B), the hydrogen shell burning becomes unstable to trigger a shell flash. The envelope structure changes from a geometrically thin configuration to a very bloated one. The photosphere expands and the photospheric temperature rapidly decreases. This is the onset of a nova outburst. The envelope mass at point B corresponds to the ignition mass, i.e., $M_{\text{ig}} = M_{\text{env}}(\text{B})$.

After the WD jumps to point C, it moves leftward as the envelope mass decreases owing to wind mass-loss and nuclear burning (Kato & Hachisu 1994; Hachisu & Kato 2001). This “stable branch” corresponds to the expanded envelope in the decay phase of nova outbursts. The photospheric radius gradually shrinks while the photospheric temperature increases. The optical brightness decays with time (Kato & Hachisu 1994; Hachisu & Kato 2006). After the optically thick winds stop at point D, the envelope mass continues to decrease owing to nuclear burning. When the WD reaches a turning point (point E), hydrogen burning becomes inactive. This is because the envelope mass is too low to support high temperature. Point E is a starting point of the unstable branch. The nuclear burning rate at point E should be the same as that of the stability line, i.e.,

$$\dot{M}_{\text{stable}} = \dot{M}_{\text{nuc}}(\text{E}), \quad (1)$$

where $\dot{M}_{\text{nuc}} = L_n/XQ$ is the nuclear burning rate, L_n is the luminosity of hydrogen burning, X is the hydrogen mass fraction, and $Q = 6.4 \times 10^{18} \text{ erg g}^{-1}$ is the energy generation per unit mass. The star quickly falls down to point A on the degenerate branch. In this way, a nova follows a limit cycle of points A, B, C, D, E, and then A.

Figure 1 also shows two other tracks for a lower ($\dot{M} \ll \dot{M}_{\text{stable}}$, dotted line) and a higher ($\dot{M} > \dot{M}_{\text{stable}}$, thin solid line) mass-accretion rates. For the lower mass-accretion rate, the degenerate branch is cooler owing to smaller gravitational energy release, but the position of the unstable branch (from point E to B) hardly changes. For this reason, point B is shifted rightward for the lower accretion rate, and hence the ignition mass is larger. For the higher mass-accretion rate, on the other hand, point B moves leftward. As a result, the ignition mass is smaller. The higher the mass-accretion rate, the narrower the limit cycle of nova outbursts.

We found that the width of this limit cycle Δ , which is de-

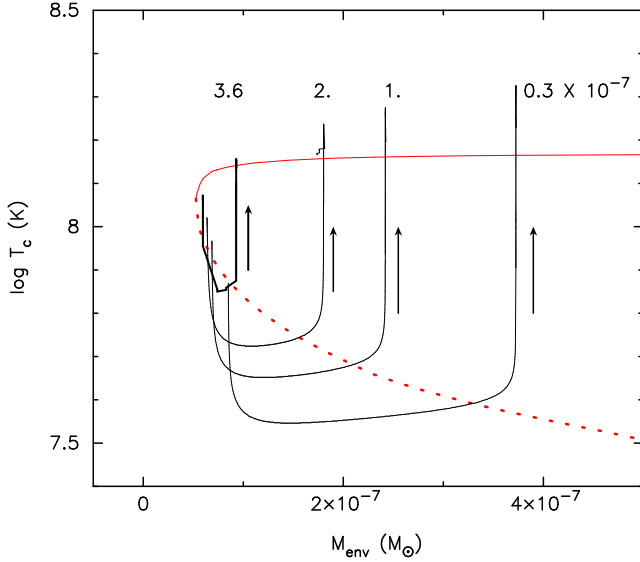


FIG. 2.— Same as Figure 1, but for time-dependent calculation on a $1.38 M_{\odot}$ WD. From left to right, the mass accretion rate is 3.6×10^{-7} (thick solid line), 2×10^{-7} , 1×10^{-7} , and $0.3 \times 10^{-7} M_{\odot} \text{ yr}^{-1}$ as attached to each curve in units of $10^{-7} M_{\odot} \text{ yr}^{-1}$. Here we define the ignition mass $M_{\text{ig}} = M_{\text{env}}$ by the envelope mass at each vertical line after the onset of the flash. Red solid and dotted lines correspond to the stable and unstable branches in Figure 1, respectively.

finied on each S-shape line by

$$\Delta = M_{\text{env}}(\text{B}) - M_{\text{env}}(\text{E}), \quad (2)$$

where $M_{\text{env}}(\text{B})$ and $M_{\text{env}}(\text{E})$ are the envelope masses at turning points B and E, respectively, does not vanish even for very high mass-accretion rates above the stability line ($\dot{M} > \dot{M}_{\text{stable}}$, thin solid line in Figure 1). In other words, the finite Δ is the reason for a finite minimum recurrence period of

$$t_{\text{rec}}^{\text{min}} = \Delta / \dot{M}_{\text{stable}}, \quad (3)$$

when the mass accretion rate increases toward the stability line, $\dot{M} \rightarrow \dot{M}_{\text{stable}}$.

Our discussion here is based on the equilibrium solutions and the tracks are slightly different from those of our time-dependent calculations as will be described in detail in Section 3. Therefore, we will identify the exact stability line by time-dependent calculation in Section 3.2.

Finally we discuss the case that the mass-accretion rate is larger than that of the stability line. In the case of thin solid line ($\dot{M} > \dot{M}_{\text{stable}}$) in Figure 1, the WD accretes hydrogen-rich matter and reaches a turning point B. Hydrogen ignites to trigger a shell flash. After the WD jumps from a turning point B to point C, it stays at a point on the stable branch right side to point E because the mass-accretion rate is larger than the nuclear burning rate at point E, i.e., $\dot{M} > \dot{M}_{\text{nuc}}(\text{E}) = \dot{M}_{\text{stable}}$. We emphasize that, after a first shell flash occurs, the WD stays at a point on the stable branch and never repeats shell flashes. We will discuss this in more detail in Section 4.2.

3. SIMULATION OF SHELL FLASHES

In this section we present and discuss results of time-evolution calculations for a part of the nova cycle. Using the equilibrium models obtained in Nomoto et al. (2007) as initial models, we followed the evolution of mass-accreting WDs. We used a Henyey type evolution code, which is the same as in Nomoto et al. (2007), except that the term proportional to $(\partial S / \partial t)_q$ with S being the specific entropy is included

to follow the evolution. The chemical composition of accreting matter and the initial hydrogen-rich envelope is assumed to be $X = 0.7$, $Y = 0.28$, and $Z = 0.02$, except in the case otherwise stated.

Using an accreting equilibrium model for the initial model of evolution is advantageous, because, after many flashes, the temperature distribution in the WD interior of a recurrent nova is expected to be similar to that of the equilibrium model accreting at the same rate. This is a good approximation, in particular, for short period recurrent novae with very high accretion rates. We assumed no helium layer between the WD core and hydrogen-rich envelope.

3.1. Ignition Mass

We obtain the ignition mass for a given WD mass and mass-accretion rate as follows: We start evolution calculation by reducing the envelope mass to a half of the corresponding equilibrium model. The nuclear luminosity, L_{n} , initially decreases because of the reduced envelope mass. This process corresponds to a falling path from a point on the unstable equilibrium branch toward the degenerate branch in Figure 1. As the envelope mass increases due to accretion, the WD moves rightward and reaches point B, at which the hydrogen burning becomes unstable and a shell flash occurs. We define the ignition mass $M_{\text{ig}} = M_{\text{env}}$ as the envelope mass at the onset of the flash. The ignition mass obtained in this way hardly depends on the process or amount of initial reduction of the envelope mass; e.g., no reduction or a 90% reduction yields similar value of M_{ig} .

Figure 2 shows evolutionary courses of such calculations for a $1.38 M_{\odot}$ WD in the $M_{\text{env}} - \log T_{\text{c}}$ diagram for some mass-accretion rates. Red dashed and solid lines are the unstable and stable branches, respectively, in Figure 1. After a steep decrease in T_{c} (and hence in the nuclear luminosity L_{n}), the envelope mass M_{env} increases to the ignition mass M_{ig} and a shell flash starts. As the shell flash sets in, the temperature T_{c} as well as the nuclear energy generation rate L_{n} increases rapidly so that the whole envelope expands. We could determine ignition mass for each case, although calculations have to be stopped at the early phase of the envelope expansion (i.e., in the early rising phase of a nova outburst), because numerical difficulties occur when the envelope is expanded. We note that, just before our calculation fails, the bottom temperature T_{c} begins to decrease toward a relaxed envelope structure of steady state which is represented by a red solid line in Figure 2.

We obtained ignition masses M_{ig} for various sets of mass accretion rate \dot{M} and WD mass M_{WD} . The results are presented by contours of M_{ig} on the $M_{\text{WD}} - \dot{M}$ plane in Figure 3. For a given \dot{M} , M_{ig} is smaller for a larger M_{WD} . For a given M_{WD} , M_{ig} is smaller for a higher \dot{M} . All contours stop at the dashed line, because above this line hydrogen shell burning is stable and no flashes occur; in other words, it is the stability line for the hydrogen shell burning. The stability line (dashed line in Figure 3) is approximately represented as

$$\dot{M}_{\text{stable}} = 4.17 \times 10^{-7} \left(\frac{M_{\text{WD}}}{M_{\odot}} - 0.53 \right) M_{\odot} \text{ yr}^{-1}. \quad (4)$$

We will discuss how the stability line is obtained in the next subsection.

The dash-dotted line in Figure 3 represents the locus of the critical accretion rate \dot{M}_{cr} above which steady models have

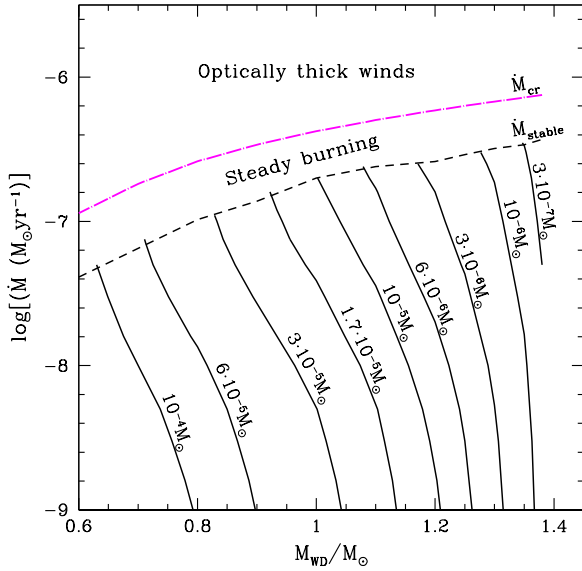


FIG. 3.— Ignition mass M_{ig} on the $M_{\text{WD}} - \dot{M}$ plane. Hydrogen burning is stable in the region above the dashed line (\dot{M}_{stable}). In the lower region to \dot{M}_{stable} , hydrogen shell burning is thermally unstable and the WD experiences shell flashes. Black solid lines indicate equi-ignition mass, the value of which is shown beside each line. Optically thick winds are accelerated in the region above the dash-dotted line (\dot{M}_{cr}).

optically thick winds (Kato & Hachisu 1994). This relation can be represented as

$$\dot{M}_{\text{cr}} = 8.18 \times 10^{-7} \left(\frac{M_{\text{WD}}}{M_{\odot}} - 0.48 \right) M_{\odot} \text{ yr}^{-1}. \quad (5)$$

3.2. Stability Line

To obtain the stability boundary of accretion rate, we start evolution calculations from an equilibrium model whose accretion rate lies well within the stable range. Then, we decrease the accretion rate slowly until a shell flash occurs. Figure 4 depicts examples for $M_{\text{WD}} = 1.35 M_{\odot}$. The initial model has a mass-accretion rate of $\dot{M} = 4.5 \times 10^{-7} M_{\odot} \text{ yr}^{-1}$. In the top panel the accretion rate \dot{M} is reduced to $3.5 \times 10^{-7} M_{\odot} \text{ yr}^{-1}$. The hydrogen shell burning is still stable at this accretion rate and the nuclear luminosity L_{n} remains nearly constant.

In the middle panel, \dot{M} is decreased to $3.4 \times 10^{-7} M_{\odot} \text{ yr}^{-1}$. The nuclear luminosity L_{n} oscillates but the amplitude is bounded. If \dot{M} is further decreased to $3.3 \times 10^{-7} M_{\odot} \text{ yr}^{-1}$, the nuclear luminosity L_{n} starts decreasing, and after certain mass is accreted a shell flash occurs (bottom panel). The stability of the hydrogen shell burning changes at $\dot{M} = 3.4 \times 10^{-7} M_{\odot} \text{ yr}^{-1}$ for $M_{\text{WD}} = 1.35 M_{\odot}$. We regard this accretion rate as the boundary of stability.

Figure 5 compares the stability line we obtained (black solid line) with those of Nomoto et al. (2007) (red dotted line) and Wolf et al. (2013) (blue dashed line). Nomoto et al. (2007) obtained the stability line from a linear perturbation analysis to equilibrium models, while Wolf et al. (2013) obtained it based on their evolution calculations. The two lines based on the time-evolution calculation agree well with each other, while the one based on the linear perturbation analysis lies below the above two lines.

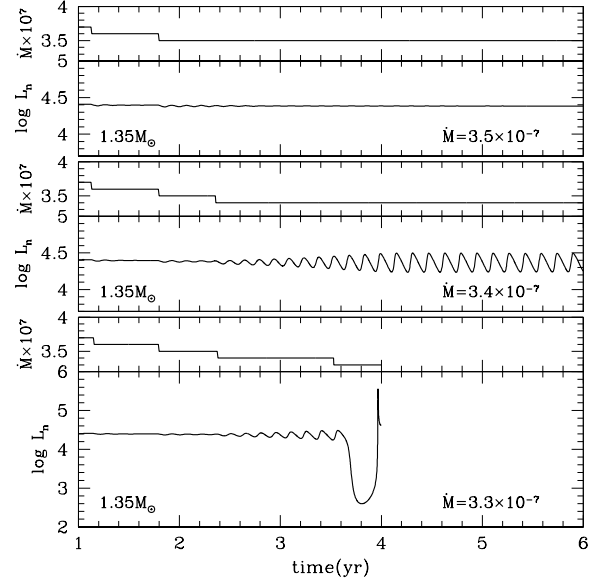


FIG. 4.— Evolutions of the nuclear luminosity, L_{n} (in units of L_{\odot}), for selected accretion rates, \dot{M} (in units of $M_{\odot} \text{ yr}^{-1}$), around the boundary between stable and unstable shell hydrogen burnings for a $1.35 M_{\odot}$ WD. Each calculation started with the equilibrium model for an accretion rate of $4.5 \times 10^{-7} M_{\odot} \text{ yr}^{-1}$, which is sufficiently high for the hydrogen shell burning to be stable. The accretion rate is gradually decreased (upper sub-panel of each panel) to $\dot{M} = 3.5 \times 10^{-7} M_{\odot} \text{ yr}^{-1}$ in the top panel, to $\dot{M} = 3.4 \times 10^{-7} M_{\odot} \text{ yr}^{-1}$ in the middle panel, and to $\dot{M} = 3.3 \times 10^{-7} M_{\odot} \text{ yr}^{-1}$ in the bottom panel. The stability of the shell burning changes at $\dot{M} = 3.4 \times 10^{-7} M_{\odot} \text{ yr}^{-1}$ (middle panel), for which the nuclear luminosity oscillates without leading to a flash. For an accretion rate slightly smaller than the above value, a shell flash occurs (bottom panel).

One of the reasons for this difference might be the fact that in the linear perturbation analysis the possibility of vibrational instability was not considered, while numerical calculations show oscillations in L_{n} (Figure 4). Another possible reason for the difference might stem from small differences in the structures between steady-state equilibrium models and evolutionary models.

3.3. Shortest Recurrence Periods

Now that we have obtained M_{ig} for various M_{WD} and \dot{M} , we can approximate the recurrence periods of novae. After a nova outburst sets in, the envelope mass of the WD decreases as its surface temperature increases. Hydrogen burning stops at point E in Figure 1 when the envelope mass reaches a local minimum, $M_{\text{env}}^{\text{min}}$. This hydrogen-rich matter remains unburnt until a next flash occurs, during this time, the amount of mass $M_{\text{ig}} - M_{\text{env}}^{\text{min}}$ is accreted. We estimate the recurrence period as $t_{\text{rec}} = (M_{\text{ig}} - M_{\text{env}}^{\text{min}}) / \dot{M}$ because the time after the ignition to point E is much shorter than the accreting time. Figure 6 shows contours of the recurrence period on the $M_{\text{WD}} - \dot{M}$ plane. The recurrence period of one year corresponding to the nova M31N 2008-12a is obtained for WDs with $(\dot{M}, M_{\text{WD}}) = (3.3 \times 10^{-7} M_{\odot} \text{ yr}^{-1}, 1.31 M_{\odot})$, $(2.4 \times 10^{-7} M_{\odot} \text{ yr}^{-1}, 1.35 M_{\odot})$, and $(1.5 \times 10^{-7} M_{\odot} \text{ yr}^{-1}, 1.38 M_{\odot})$. For a given \dot{M} , the recurrence period is shorter for a larger M_{WD} . For a given M_{WD} , the recurrence period is shorter for a higher \dot{M} . The latter is limited by the stability line as indicated by the dashed line in Figure 6, which gives a lower bound of the recurrence period for a given M_{WD} . We should

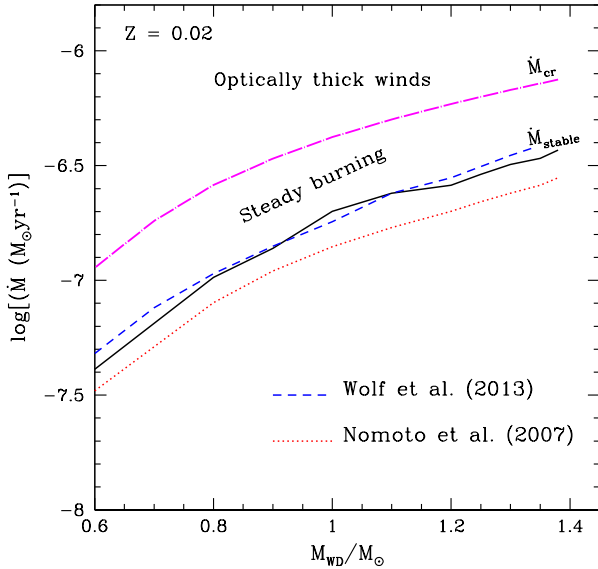


FIG. 5.— Comparison of the stability line calculated by this work (black solid line) with Nomoto et al. (2007) (red dotted line) and Wolf et al. (2013) (blue dashed line) in the $M_{\text{WD}}-\dot{M}$ diagram. Other symbols/lines are the same as those in Figure 3. See Section 3.2 for detail.

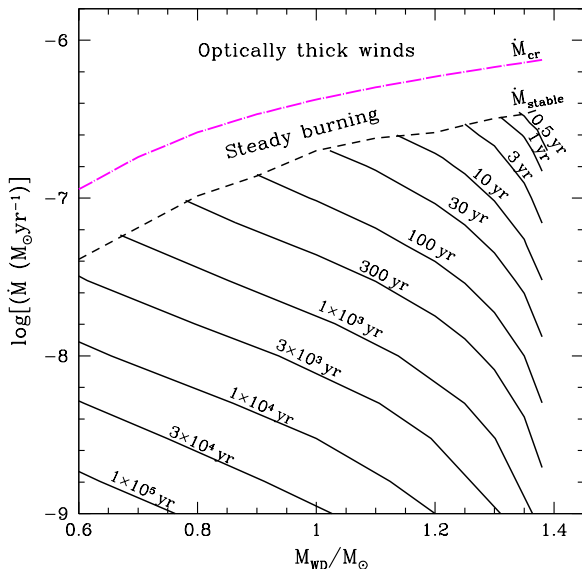


FIG. 6.— Recurrence period t_{rec} of novae on the $M_{\text{WD}}-\dot{M}$ plane. We plot loci of equi-recurrence period of novae (black solid lines). Other symbols/lines are the same as in Figure 3.

note that for the accretion rate as high as $\dot{M} > 10^{-7} M_{\odot} \text{ yr}^{-1}$ encountered here, the accreting C+O WD becomes an SN Ia when M_{WD} reaches $1.38 M_{\odot}$ by igniting a carbon deflagration at the center of the WD (Nomoto 1982; Nomoto et al. 1984). If the accreting WD is an O+Ne+Mg WD, electron capture triggers a collapse when $M_{\text{WD}} = 1.38 M_{\odot}$ (Nomoto 1984). Therefore, the *shortest* recurrence period of novae is obtained for the $1.38 M_{\odot}$ WD with the accretion rate of $3.6 \times 10^{-7} M_{\odot} \text{ yr}^{-1}$, which is found to be about 2 months (see Figure 8 below).

4. DISCUSSION

4.1. Comparison with Other Works: Under the Stability Line

Prialnik & Kovetz (1995) calculated shell flashes for various WD masses and accretion rates. For $\dot{M} = 1 \times 10^{-7} M_{\odot} \text{ yr}^{-1}$ with a core temperature of $T_c = 5 \times 10^7 \text{ K}$, they obtained the WD mass, accreted mass, and recurrence period as ($1.0 M_{\odot}$, $8.30 \times 10^{-6} M_{\odot}$, 83 yr), ($1.25 M_{\odot}$, $1.96 \times 10^{-6} M_{\odot}$, 19.6 yr), and ($1.4 M_{\odot}$, $8.09 \times 10^{-8} M_{\odot}$, 0.809 yr). Idan et al. (2013) reported that, for the same accretion rate of $1 \times 10^{-7} M_{\odot} \text{ yr}^{-1}$, ($1.0 M_{\odot}$, $9 \times 10^{-6} M_{\odot}$, 100 yr), ($1.25 M_{\odot}$, $1.5 \times 10^{-6} M_{\odot}$, 16 yr), ($1.35 M_{\odot}$, $3.5 \times 10^{-7} M_{\odot}$, 3.7 yr), and ($1.4 M_{\odot}$, $5 \times 10^{-8} M_{\odot}$, 0.5 yr). Our models yield ($1.0 M_{\odot}$, $1.3 \times 10^{-5} M_{\odot}$, 95 yr), ($1.25 M_{\odot}$, $2.3 \times 10^{-6} M_{\odot}$, 17 yr), ($1.35 M_{\odot}$, $5.5 \times 10^{-7} M_{\odot}$, 4.2 yr), and ($1.38 M_{\odot}$, $2.4 \times 10^{-7} M_{\odot}$, 1.8 yr). These values are more or less consistent with each other. In our model, the WD is heated up by gravitational energy release due to high mass-accretion rates. As a result, the WD radius (i.e., the bottom of the envelope) should be slightly larger than those of Idan et al. (2013) and Prialnik & Kovetz (1995). Thus, our envelope mass is larger than theirs, because of a smaller surface gravity of the WD.

Wolf et al. (2013) calculated shell flashes on a $1.0 M_{\odot}$ WD with $\dot{M} = 1 \times 10^{-9} M_{\odot} \text{ yr}^{-1}$ and obtained the mass of the hydrogen-rich envelope with $X > 0.1$ is $5 \times 10^{-5} M_{\odot}$. Our value $M_{\text{ig}} = 3.9 \times 10^{-5} M_{\odot}$ is slightly smaller than theirs, which can be explained as a difference of the inner boundary condition. Our model includes gravitational energy release from a hotter WD core edge, thus giving a smaller ignition mass, whereas Wolf et al.'s model has cooler WD core edge because of the absence of a hot helium layer, thus yielding a larger ignition mass. For high mass accretion rates near the stability line, our ignition mass M_{ig} is very consistent with Wolf et al.'s results, as indicated by the agreement of the two stability lines in Figure 5. For high mass-accretion rates, Wolf et al.'s model develops a hot helium layer below the accreted hydrogen-rich envelope after the WD experiences several shell flashes. Wolf et al. claimed that the presence of the hot helium layer is essentially important for nova outbursts of short recurrence periods, because the hot helium layer act as a heat reservoir even if the WD is cool. Our model has no helium layer but has a hot WD core, which is heated up by compressional heating due to high mass-accretion rates. Therefore, ours and Wolf et al.'s model have essentially the same boundary condition in view of the heat reservoir at the bottom of hydrogen-rich envelope, thus giving the very consistent results.

4.2. Shell Flashes above the Stability Line: Artifact Flashes

Although the stability line of shell flashes in Figure 3 has long been established (Iben 1982; Sion et al. 1979; Nomoto et al. 2007; Wolf et al. 2013), some numerical calculations showed repeated shell flashes for accretion rates even above the stability line (Kovetz & Prialnik 1994; Prialnik & Kovetz 1995; Starrfield et al. 2012; Idan et al. 2013). In these cases, the recurrence period is much shorter than our minimum value and the light curves show very high duty cycle. For example, Kovetz & Prialnik (1994) reported the calculation of several successive shell flashes on a $1.4 M_{\odot}$ WD with $\dot{M} = 1 \times 10^{-6} M_{\odot} \text{ yr}^{-1}$. The bolometric luminosity varies between $\log(L_{\text{bol}}/L_{\odot}) \sim 3.7$ and ~ 4.8 , and the bright stage lasts 10 days, almost a half of the recurrence pe-

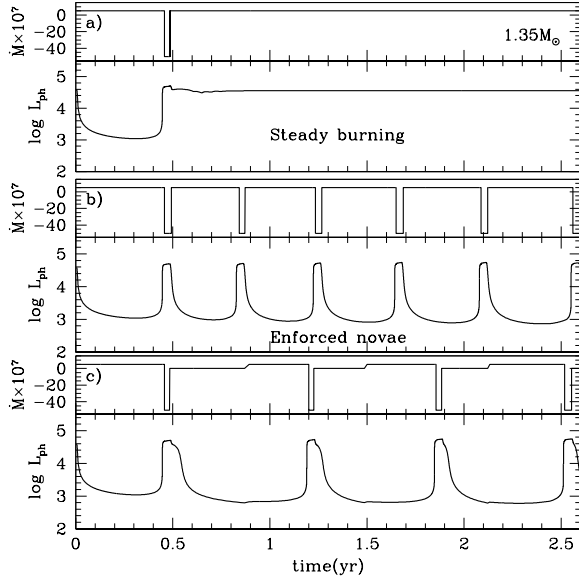


FIG. 7.— Evolutions of the photospheric luminosity, $\log L_{\text{ph}}$ (in units of L_{\odot}), of a $1.35 M_{\odot}$ WD for an accretion rate of $\dot{M} = 5 \times 10^{-7} M_{\odot} \text{ yr}^{-1}$, above the stability line. Each calculation started with about a half of the equilibrium mass and, therefore, underwent a first shell flash at about 0.45 yr. To avoid numerical difficulty, we assume an artificial wind mass-loss of $\dot{M} = -5 \times 10^{-6} M_{\odot} \text{ yr}^{-1}$ when the photosphere expands to $\log R_{\text{ph}}/R_{\odot} > -1.7$. In the upper part of each panel, we plot our control mass-accretion/mass-loss rate in units of $10^{-7} M_{\odot} \text{ yr}^{-1}$. (a) Upper panel: after a first shell flash, we stopped the wind mass-loss and restarted mass accretion when the photospheric radius shrank to $\log R_{\text{ph}}/R_{\odot} = -2.0$, where the envelope did not reach point E in Figure 1 yet. Hydrogen burning is going on (steady state). The envelope stays on the stable branch in Figure 1. (b) Middle panel: after a first shell flash, we stopped the wind mass-loss and restarted mass accretion when the photospheric radius shrank to $\log R_{\text{ph}}/R_{\odot} = -2.4$, where the envelope already reached point E in Figure 1 and began to fall down toward point A. The envelope repeats a limit cycle (enforced novae). (c) Bottom panel: after a first shell flash, we stopped the wind mass-loss when the photospheric radius shrank to $\log R_{\text{ph}}/R_{\odot} = -2.0$, but did not restart mass accretion, i.e., $\dot{M} = 0$, until the photospheric luminosity decreases to $\log L_{\text{ph}}/L_{\odot} < 2.8$. The envelope gradually moved to and reached point E in Figure 1. After the envelope fell down toward point A, we restarted mass accretion. The envelope again underwent a shell flash (enforced novae). The recurrence time is longer than the case of middle panel.

riod of 20 days. Iban et al. (2013) obtained successive nova outbursts for a $1.0 M_{\odot}$ WD with the mass accretion rate of $1 \times 10^{-6} M_{\odot} \text{ yr}^{-1}$. The bright stage lasts 6 yr, 60% of the total recurrence period of 10 yr. Both of these calculations show a long-lasting high luminosity phase during the relatively short recurrence period. Such light curves do not resemble those of recurrent novae that show much shorter duty cycles.

The accretion rate of $\dot{M} = 1 \times 10^{-6} M_{\odot} \text{ yr}^{-1}$ corresponds to the region above the stability line in Figure 3, in which hydrogen shell burning should be stable as already discussed in Section 2 (Figure 1). Nevertheless, these papers reported successive nova outbursts. This is because they stopped accretion during the shell flashes. Without supply of hydrogen (nuclear fuel), a nova evolves toward point E in Figure 1 where it immediately falls down to point A. These authors then restarted accretion. After some time, the next shell flash begins and it goes up from point B to point C. In this way, these authors switched on and off mass-accretion to run the limit cycle. In other words, these outbursts are ‘enforced novae’ and it is not known whether such on/off switch works in nova outbursts or in other accreting binaries.

Figure 7 shows the examples of our numerical simulations for such enforced novae for a $1.35 M_{\odot}$ WD with an accretion rate of $\dot{M} = 5 \times 10^{-7} M_{\odot} \text{ yr}^{-1}$, which is above the stability line. We show three cases for different on/off switch of mass accretion. Each calculation started with about a half of the equilibrium envelope mass and, therefore, the envelope undergoes a first shell flash at about 0.45 yr. To avoid numerical difficulty, we assumed an artificial wind mass-loss of $\dot{M} = -5 \times 10^{-6} M_{\odot} \text{ yr}^{-1}$ when the photosphere expands greatly ($\log R_{\text{ph}}/R_{\odot} > -1.7$). (a) Upper panel: after a first shell flash, we stopped the wind mass-loss when the photospheric radius shrank to $\log R_{\text{ph}}/R_{\odot} = -2.0$ and immediately restarted mass accretion, where the envelope did not yet reach point E in Figure 1. Hydrogen burning is going on (steady state). The envelope stays on the stable branch in Figure 1. In the upper part of each panel, we plot our control mass-accretion/mass-loss rate in units of $10^{-7} M_{\odot} \text{ yr}^{-1}$. (b) Middle panel: after a first shell flash, we stopped the wind mass-loss and immediately restarted mass accretion when the photospheric radius shrank to $\log R_{\text{ph}}/R_{\odot} = -2.4$, which is a bit later than the case of (a). The envelope had already passed through point E in Figure 1 and fell down toward point A. After we restarted mass accretion, the envelope repeated a limit cycle. This is the enforced nova outburst. (c) Bottom panel: after a first shell flash, we stopped the wind mass-loss when the photospheric radius shrank to $\log R_{\text{ph}}/R_{\odot} = -2.0$, the same time as in the case of (a), but did not restart mass accretion, i.e., $\dot{M} = 0$, until the photospheric luminosity further decreases to $\log L_{\text{ph}}/L_{\odot} < 2.8$. We restarted mass accretion after the envelope fell down from point E toward point A in Figure 1. The envelope again underwent a shell flash (enforced novae). The recurrence time is longer than the case of middle panel because we delayed the restart of mass-accretion. In this way, we can control the recurrence period by changing the restarting time of mass-accretion. The above three cases clearly show that shell flashes above the stability line are just artifacts that stem from the numerical treatment of on/off switch of mass accretion.

There is some indication that accretion does not stop in real binaries. When the accretion rate is between the two lines of \dot{M}_{cr} and \dot{M}_{stable} in Figure 3, the WD burns hydrogen at the same rate as the accretion rate and stays somewhere between point D and point E in Figure 1. These binaries correspond to steady SSSs like CAL 83, 1E0035.4–7230, and RX J0925.7–4758 (e.g., van den Heuvel et al. 1992; Nomoto et al. 2007). In these binaries the WD is considered to accrete matter from the disk and to emit X-rays from the other WD surface area.

If the accretion rate is larger than \dot{M}_{cr} , the star stays somewhere right side to point D in Figure 1, in which the optically thick winds occur. The mass accretion rate is balanced with the sum of the nuclear burning rate and the wind mass-loss rate. In such a case, the WD accretes matter from the disk and ejects excess matter in the wind from the other region. RX J0513.9–6951 and V Sge are considered to be such objects (Hachisu & Kato 2003a,b).

4.3. Effects of Chemical Composition

The ignition mass depends on the chemical composition of the envelope as well as the WD mass and the mass accretion rate. Figure 8 compares the ignition mass and the recurrence period for $X = 0.1$, $Y = 0.88$, and $Z = 0.02$ with those of the solar composition. The ignition mass for $X = 0.1$ is system-

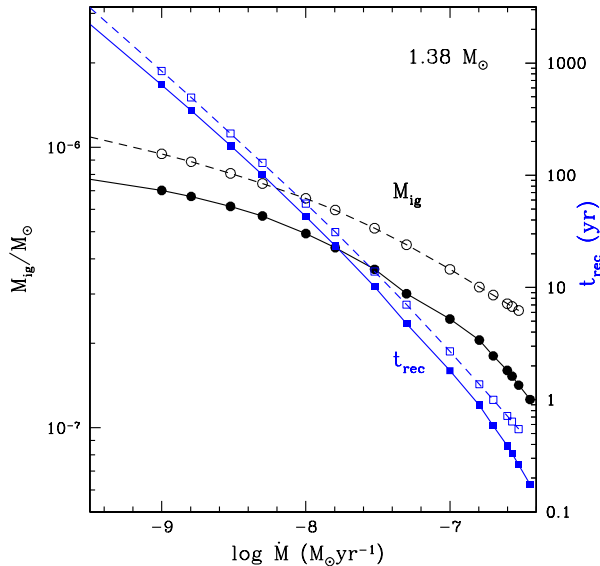


FIG. 8.— Recurrence period and ignition mass of novae on a $1.38 M_{\odot}$ WD. Black lines/symbols are for ignition masses, for which the left vertical axis should be referred. Blue lines/symbols are for recurrence times t_{rec} (right vertical axis). Solid lines with filled symbols indicate the case of $X = 0.7$, $Y = 0.28$, and $Z = 0.02$, whereas dashed lines with open symbols of $X = 0.1$, $Y = 0.88$, and $Z = 0.02$. The minimum recurrence period is about two months for the case of $X = 0.7$, $Y = 0.28$, and $Z = 0.02$.

atically larger than that for $X = 0.7$. The nuclear burning rate due to pp -chain is proportional to X^2 and the rate of CNO cycle is proportional to X . For smaller X , unstable nuclear

burning ignites at a higher temperature T_c , which results in a more massive envelope. This will be useful to binary evolution calculation toward SNe Ia, in which a WD accretes He-rich matter (suggested for U Sco type binaries, Hachisu et al. 1999a).

5. CONCLUSION

The main results are summarized as follows.

1. We proposed a physical mechanism that leads to a finite minimum recurrence period of novae.
2. We calculated the ignition masses for various WD masses and mass-accretion rates. We identified that the shortest recurrence period of novae is about two months for a non-rotating $1.38 M_{\odot}$ WD with the mass-accretion rate of $3.6 \times 10^{-7} M_{\odot} \text{ yr}^{-1}$.
3. One year recurrence period of a nova is possible only for very massive WDs ($M_{\text{WD}} \gtrsim 1.3 M_{\odot}$) and for very high mass-accretion rates, e.g., $\dot{M} = 3.3 \times 10^{-7} M_{\odot} \text{ yr}^{-1}$ for a $1.31 M_{\odot}$ WD, $2.4 \times 10^{-7} M_{\odot} \text{ yr}^{-1}$ for a $1.35 M_{\odot}$ WD, and $1.5 \times 10^{-7} M_{\odot} \text{ yr}^{-1}$ for a $1.38 M_{\odot}$ WD.
4. We present a revised stability limit of hydrogen shell burning that will be useful for binary evolution calculation toward Type Ia supernovae.

This research was supported in part by the Grants-in-Aid for Scientific Research (22540254 and 24540227) from the Japan Society for the Promotion of Science.

REFERENCES

- Darnley, M. J., Williams, S. C., Bode, M. F., et al. 2014, *A&A*, in press (arXiv:1401.2905)
- Eggleton, P., Faulkner, J., & Flannery, P. 1973, *A&A*, 23, 325
- Hachisu, I., & Kato, M. 2001, *ApJ*, 558, 323
- Hachisu, I., & Kato, M. 2003a, *ApJ*, 590, 445
- Hachisu, I., & Kato, M. 2003b, *ApJ*, 598, 527
- Hachisu, I., & Kato, M. 2006, *ApJS*, 167, 59
- Hachisu, I., Kato, M., Nomoto, K., & Umeda, H. 1999a, *ApJ*, 519, 314
- Hachisu, I., Kato, M., & Nomoto, K. 1999b, *ApJ*, 522, 487
- Hachisu, I., Kato, M., & Nomoto, K. 2010, *ApJ*, 724, L212
- Han, Z., & Podsiadlowski, Ph. 2004, *MNRAS*, 350, 1301
- Henze, M., Ness, J.-U., Darnley, M., et al. 2014, *A&A*, in press (arXiv:1401.2904)
- Iben, I. Jr. 1982, *ApJ*, 259, 244
- Idan, I., Shaviv, N. J., & Shaviv, G. 2013, *MNRAS*, 433, 2884
- Iglesias, C. A., & Rogers, F. J. 1996, *ApJ*, 464, 943
- Kato, M. 1980, *Progress of Theoretical Physics*, 64, 847
- Kato, M. 1982, *PASJ*, 34, 173
- Kato, M. 1983, *PASJ*, 35, 507
- Kato, M., & Hachisu, I. 1994, *ApJ*, 437, 802
- Kato, M., & Hachisu, I. 2012, *BASI*, 40, 393
- Kovetz, A., & Prialnik, D. 1994, *ApJ*, 424, 319
- Neo, S., Miyaji, S., Nomoto, K., & Sugimoto, D. 1977, *PASJ*, 29, 249
- Nomoto, K. 1982, *ApJ*, 253, 798
- Nomoto, K. 1984, *ApJ*, 277, 791
- Nomoto, K., Saio, H., Kato, M., & Hachisu, I. 2007, *ApJ*, 663, 1269
- Nomoto, K., Thielemann, F.-K., & Yokoi, K. 1984, *ApJ*, 286, 644
- Prialnik, D., & Kovetz, A. 1995, *ApJ*, 445, 789
- Sienkiewicz, R. 1975, *A&A*, 45, 411
- Sienkiewicz, R. 1980, *A&A*, 85, 295
- Sion, E. M., Acierno, M. J., & Tomczyk, S. 1979, *ApJ*, 230, 832
- Starrfield, S., Iliadis, C., Timmes, F. X., et al. 2012, *BASI*, 40, 419
- Tang, S., Bildsten, L., Wolf, W. M., et al. 2014, *ApJ*, in press (arXiv:1401.2426)
- van den Heuvel, E. P. J., Bhattacharya, D., Nomoto, K., & Rappaport, S. 1992, *A&A*, 262, 97
- Wolf, W. M., Bildsten, L., Brooks, J., & Paxton, B. 2013, *ApJ*, 777, 136